Heliyon

Received:
24 September 2018
Revised:
2 December 2018
Accepted:
18 December 2018

Cite as: Reda Hassanien, Dalal Z. Husein, Mostafa F. Al-Hakkani. Biosynthesis of copper nanoparticles using aqueous *Tilia* extract: antimicrobial and anticancer activities. Heliyon 4 (2018) e01077. doi: 10.1016/j.heliyon.2018.e01077

Biosynthesis of copper nanoparticles using aqueous *Tilia* extract: antimicrobial and anticancer activities

Reda Hassanien*, Dalal Z. Husein, Mostafa F. Al-Hakkani

Chemistry Department, Faculty of Science, New Valley University, El-Kharja 72511, Egypt

* Corresponding author.

E-mail address: Reda.h@scinv.au.edu.eg (R. Hassanien).

Abstract

A cost-effective method for the biosynthesis of copper nanoparticles (Cu-NPLs) using *Tilia* extract under optimum conditions has been presented. The use of *Tilia* extracts for the synthesis of Cu-NPLs has been investigated for the first time. The Cu-NPLs are stable due to *in situ* bio-capping by the *Tilia* extract residues. Formation of metallic Cu was revealed by UV-vis and XRD analyses. UV-vis of Cu-NPLs showed an SPR characteristic peak at 563 nm (energy bandgap = 2.1 eV). Morphology and size of the as-prepared Cu-NPLs were determined using SEM and TEM studies. TEM observations show that the produced Cu-NPLs are hemispherical in shape with different diameters in the range 4.7−17.4 nm. The electrical conductivity of the Cu-NPLs was determined as 1.04×10^{-6} S cm^{-1} (at T = 120 K). The antimicrobial studies exhibited relatively high activity against pathogenic bacteria like Gram-positive & Gram-negative bacteria. Anticancer studies demonstrated the *in vitro* cytotoxicity value of Cu-NPLs against tested human colon cancer Caco-2 cells, human hepatic cancer HepG2 cells and human breast cancer Mcf-7 cells. To conclude, Cu-NPLs are promising in electronic devices and they possess a potential anticancer application for some human cancer therapy as well.

Keywords: Materials science, Materials chemistry, Nanotechnology

https://doi.org/10.1016/j.heliyon.2018.e01077

1. Introduction

The unique properties of nanoparticles have given progress to tremendous research activity directed toward nanoparticle preparation and applications [1, 2, 3, 4]. Copper nanoparticles (Cu-NPLs) have important applications in diverse fields such as catalysis [5, 6, 7], water treatment [8], information storage and solar cells [9]. Cu-NPLs in comparison with the bulk Cu are suitable materials for use in printed electronics and good substitutes for conductive ink to manufacture low-cost electronic components by ink-jet printing [10, 11]. In addition, copper plays a significant role in the advanced electronic circuit due to its admirable electrical conductivity and relatively low costs. Cu-NPLs have also been used as disinfectants due to their antibacterial properties [12]. Furthermore, Cu-NPLs are potentially applied in the pharmaceutical, health care and environmental health.

Different methodologies have been employed to fabricate the nanoparticle with controllable properties such as shape and size; these include vapor deposition [13], electrochemical reduction [14], thermal decomposition [12, 15] and chemical reduction of copper salts [16, 17, 18, 19]. Although numerous chemical methods have been used to produce Cu-NPLs, the use of toxic chemicals in the production of Cu-NPLs limits their pharmaceutical and medical applications [20]. Biosynthesis of pure and stable Cu-NPLs is a challenging task as they undergo rapid oxidation in air or aqueous media [21, 22], even after preservation in an inert atmosphere e.g., Ar or N_2.

The advancement of "*green chemistry*" approach over chemical and physical methods are easy to control of the reaction process, high production rate, cost-effective and environmentally friendly whereas harmful chemicals, high-temperature, energy, and pressure are not required for the green synthesis [23, 24, 25]. Thus, the preparation of Cu-NPLs using plant extracts has attracted great attention because of the availability of biological entities, diversity and eco-friendly procedures [25, 26, 27]. Plant extracts contain natural compounds, e.g., alkaloids, flavonoids, steroids and other nutritional compounds [28]. In this way, the plant extracts can act as strong natural reducers and stabilizers. Although the biosynthesis of Cu-NPLs by plants has been reported, the potential of other plants for the green synthesis of Cu-NPLs is yet to be fully explored.

To the best of our knowledge, the use of *Tilia* extracts for the synthesis of Cu-NPLs has not been reported so far. *Tilia* plant extracts are rich in functional molecules such as flavonoids and phenolic compounds which have been regarded as powerful natural reducing and capping agents [29]. Hence, the basic principle of our method for the synthesis of Cu-NPLs is the reduction of copper ions by *Tilia* plant extracts. In this work, a fast and convenient method to produce non-oxidative Cu-NPLs by

https://doi.org/10.1016/j.heliyon.2018.e01077

biologically reducing Cu ions with an aqueous extract of *Tilia* under optimum conditions is described. The properties of the Cu particles were characterized using different techniques (FTIR, UV-vis, XRD, SEM, and TEM). The antibacterial, antifungal and anticancer activities of the Cu-NPLs are also discussed.

2. Materials and methods

2.1. Chemicals

All the chemicals, used in this experiment, were analytical grade and used as purchased without further purification. Copper (II) sulfate pentahydrate salt, $CuSO_4 \cdot 5H_2O$, of 99 % purity (Merck), was dissolved in deionized water.

2.2. Preparation of the aqueous *Tilia* extract

The fresh matured leaves of *Tilia* were collected and washed with deionized water. About 100 g of dried leaves were crushed and heated with 500 ml of deionized water. The mixture was heated to boiling for 5 h under a reflux system and reduced pressure in a rotary evaporator to produce a dark brown color extract. Then the mixture was cooled and centrifuged at 12000 rpm and filtered through Whatman No.1 filter paper. The produced filtrate was freshly used.

2.3. Synthesis and isolation of Cu-NPLs

In 500 ml beaker, the *Tilia* aqueous extract was added to copper sulfate pentahydrate solution (4:1 v/v) and the mixture was heated to 80 °C with a continuous stirring for 25 min. The mixture was left in the dark for 24 h to settle. The mixture was purified by repeating centrifugation at 6000 rpm for 5 min (3 times) and then dispersed the buff precipitate with deionized water to remove any residual of the biological extract, then the buff precipitate was washed with ethanol several times. Finally, the precipitate was put it in an oven for 2 h for drying at 100 °C.

2.4. Antitumor efficacy in vitro using cancer cell lines; Caco-2, HepG2, and Mcf-7 cells

2.4.1. Cell viability test (MTT assay)

Cell viability was determined using the MTT assay. MTT (3-[4,5-dimethylthiazol-2-yl]-2,5-diphenyltetrazolium bromide) is a water-soluble tetrazolium salt converted to formazan (an insoluble purple color) by the cleavage of the tetrazolium ring through the succinate dehydrogenase within the mitochondria. Since the cell membranes are impermeable to the formazan product, the product accumulates in healthy cells. Formazan levels were quantified by measuring the absorbance at 560 nm using a

https://doi.org/10.1016/j.heliyon.2018.e01077

microplate reader. The optical density of formazan formed in untreated control cells was taken as 100 % viability. The obtained optical densities from the treated wells were converted to a percentage of living cells against the control [30]. Different concentrations of Cu-NPLs were used (1000−1.95 μg/mL). For calculation of IC50, both viability % and toxicity % were determined.

2.4.2. Cell culture

The cell lines used in the present study were human colorectal adenocarcinoma Caco-2 cells, human hepatocellular carcinoma HepG2 cells, and human breast cancer Mcf-7 cells. The cell lines were purchased from VacSERA, Egypt. The cells were cultured in RPMI medium, including 10 % fetal bovine serum (FBS), sodium bicarbonate, L-glutamine 1 % (v/v), 1 % (v/v) penicillin-streptomycin solution and 7.5 % $NaHCO_3$. The cells were maintained at 37 °C in a humidified atmosphere of 5 % CO_2 and 95 % air.

2.4.3. MTT protocol

Cells were seeded in 96-well microplates and routinely cultured in a humidified incubator for 24h. This assay was performed in triplicate. The 96 well tissue culture plate was inoculated with 1×10^5 cells/mL (100 μl/well) and incubated at 37 °C for 24 h to develop a complete monolayer sheet. The growth medium was decanted from 96 well microplates after confluent sheet of cells were formed; cell monolayer was washed twice with wash media. Twofold dilutions of the tested sample were made in RPMI medium with 2 % serum (maintenance medium). Then 0.1 mL of each dilution was tested in different wells, leaving 3 wells as a control, receiving only maintenance medium. The plate was incubated at 37 °C and examined. MTT solution was prepared (5 mg/ml in PBS). The 20 μl MTT solution was added to each well. Place on a shaking table, 150 rpm for 5 min to thoroughly mix the MTT into the media. Incubation (37 °C, 5 % CO_2) for 1−5 h was done to allow the MTT to be metabolized. Dump off the media. Resuspend formazan in 200μl DMSO. Place on a shaking table, 150 rpm for 5 min to thoroughly mix the formazan into the solvent. Optical density (OD) was read at 560 nm. The limitation of the present study is the lack of studies of the underlying molecular mechanisms for the anticancer activity and toxicology studies.

2.5. Determination of the antimicrobial activity of Cu-NPLs

The antimicrobial activity of the biosynthesized Cu-NPLs was determined by using the well diffusion method. The bacteria used for the antibacterial activity were *Pseudomonas aeruginosa* ATCC 9027, *Escherichia coli* ATCC 8739 represented Gram-negative bacteria while *Bacillus subtilis* ATCC 6633, *Staphylococcus aureus* ATCC

https://doi.org/10.1016/j.heliyon.2018.e01077

6538P represented Gram-positive bacteria. Furthermore, *Candida albicans* ATCC 10231 represents a pathogenic fungal strain. All the bacterial and fungal cultures were provided from the Assiut University Mycological Centre (AUMC), Assiut, Egypt. For positive control, Cefipime was used as a standard antibacterial agent, while, DMSO was used as a solvent. A 50 μL of four different concentrations of Cu-NPLs solutions were prepared; 25, 50,100 and 200 μg/mL and poured into the wells, then incubated at 37 °C for 24 h. For the reference antibiotic, 150 μg/ml was used in the present study. In the first stage, different concentrations of Cu-NPLs in DMSO were used for different types of Gram-positive & Gram-negative bacteria and pathogenic yeast. Secondly, tests were done against antimicrobial as a standard (positive control) (Cefepime hydrochloride monohydrate L-arginine) and antifungal standard (Fluconazole) with the comparison to the negative control test of the aqueous liquid extract of *Tilia* and DMSO solvent.

2.5.1. Culture media were prepared as follows

Mueller-Hinton Agar (MHA) (Oxoid) was used for the cultivation of bacterial strains. Composition (g/L): Beef, dehydrated infusion from, 2; Agar, 15; Casein hydrolysate, 17.5 and starch, 1.5 (pH 7.3 ± 0.2). The medium was sterilized by autoclaving at 121 °C for 15 min. Sabouraud Dextrose Agar (SDA) (Oxoid) was used for cultivation of *C. albicans*. Composition (g/L): Mycological peptone, 10; Agar, 15 and glucose, 40 (pH 5.6 ± 0.2). The medium was sterilized by autoclaving at 121 °C for 15 min and then it was mixed well and poured into sterile Petri dishes.

2.6. Sample characterization

1 Infrared spectra were recorded on a Thermo Fisher (model: Nicolet iS10 FT-IR spectrometer) in a wave number range 4500−500 cm^{-1}.

2 The UV-vis absorption spectra measurements of the Cu-NPLs were recorded in the range 200−900nm by PerkinElmer; model: LAMBDA 750 UV/Vis/NIR Spectrophotometer. The synthesized Cu-NPLs powder sample was dispersed in DMF and optical characterizations were executed.

3 The structure of the nanoparticles was investigated by a Philips X-ray diffractometer (model PW 1710).

4 The morphology of the Cu-NPLs was investigated by scanning electron microscopy (SEM; JEOL [model: JSM 5400LV]) and transmission electron microscopy (TEM; JEOL [model: JEM-100 CXII]).

5 The resistance was measured using a high resistance meter (Keithley, Model 6517B) with a range of 103−1013 Ω.

https://doi.org/10.1016/j.heliyon.2018.e01077

3. Results and discussion

3.1. FTIR study

The presence of active phenolic compounds like flavonoids in the *Tilia* extract before and after the bio-reduction process was identified by FTIR. The *Tilia* extract displays many absorption peaks, reflecting its complex nature [29]. On the one hand, the FTIR spectrum of aqueous extract of the *Tilia* (Fig. 1; black) shows five main peaks at 3419, 2952, 1760, 1688 and 1141 cm^{-1} which represent O-H stretching vibrations (alcoholic or phenolic), C−H asymmetric stretching, C=O stretching, C=C stretching and C−OH bending, respectively. Flavonoid and phenolic acids could be adsorbed on the surface of Cu-NPLs, possibly by the interaction through π−electrons interaction [31]. The carbonyl and hydroxyl linkages in the *Tilia* extract's components are responsible for the reduction of copper ions to Cu-NPLs. On the other hand, the FTIR spectrum of green-synthesized Cu-NPLs (Fig. 1; red) shows a broad peak in 3410 cm^{-1} due to O-H groups, also some signals emerged in 2949, 1783, 1615 and 1028 cm^{-1} are related to C−H asymmetric stretching, C=O of aromatic rings, C=C stretching and C−OH bending, respectively. FTIR spectrum of Cu-NPLs also reveals the possible interaction between Cu ions and *Tilia* extract during the bioreduction stage. The presence of characteristic vibration of Cu_2O is not observed [32, 33] at 621 cm^{-1}.

By comparing the spectrum of Cu-NPLs with that of the *Tilia* extract, it was found that some peaks obtained from the plant extract have been repeated in the FTIR spectrum of Cu-NPLs with slight changes in the band positions as well as the intensities of the absorption. These results show that the as-synthesized Cu-NPLs are non-oxidative, pure and coated with *Tilia* extract components.

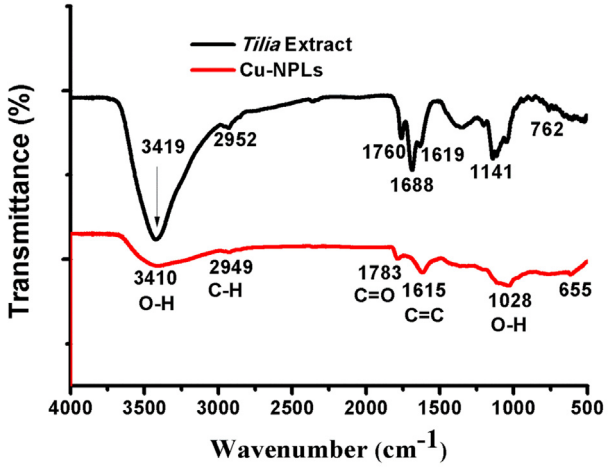

Fig. 1. FTIR spectra of aqueous *Tilia* extract (black curve) and Cu-NPLs (red curve) in a wave number range 4500−500 cm^{-1}. The FTIR spectra revealed the reducing, capping and stabilizing capacity of the plant extract. The spectra are offset for clarity.

https://doi.org/10.1016/j.heliyon.2018.e01077

3.2. Optical study

Initially, Cu-NPLs were confirmed by the change of color after addition of *Tilia* extract into the Cu^{2+} solution due to the surface plasmon resonance (SPR) phenomenon. The free electrons or conduction electrons can couple with the visible light when the given plasmonic mode matches the energy of an incident photon. The blue color of the Cu^{2+}solution changed to dark brown around 563nm (Fig. 2A); the Cu^{2+} has no such peak, indicating the formation of Cu^{0} as characterized by the absorption spectroscopy.

Tunable SPR is important to find out the diverse applications of Cu-NPLs. UV-vis spectrum of Cu-NPLs suspension as the function of wavelength was recorded at room temperature in the range of 550−585 nm (Fig. 2A**).** Obviously, Cu (II) showed a broad band from 600 to 800 nm in the visible region, which disappeared by adding the *Tilia* extract. The spectrum also displays the SPR characteristic peak at 563 nm for metallic copper [34]. The broadness of the absorption band can be attributed to the polycrystalline nature of Cu nanoparticles as is clearly observed from XRD analysis. Thus, the Cu-NPLs obtained here are stable due to *in situ* bio-capping by the *Tilia* extract residue. The stability of the Cu-NPLs was checked at regular intervals (3 days) by observing the presence of the SPR peak in the optical spectrum. These Cu-NPLs show an exceptional stability: they can be preserved for over a month without considerable oxidation and for this preservation purging of N_2 gas is unnecessary.

The dependence of the optical absorption coefficient (α) on photon energy helps to analyze the band structure and the type of transition of electrons. The absorption coefficient (α) at the corresponding wavelength λ is calculated using the Beer-Lambert's relation (Eq. 1) [35].

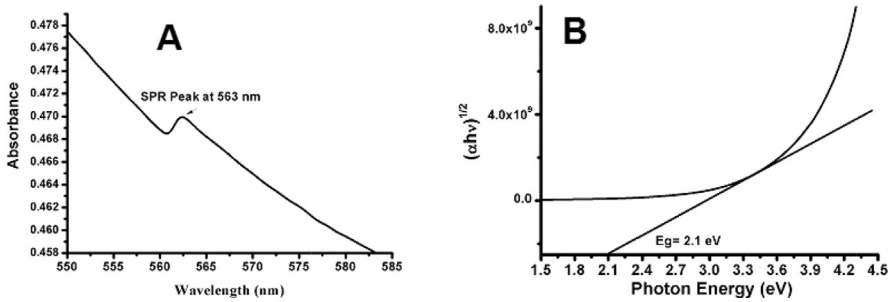

Fig. 2. UV-vis absorption spectrum of Cu-NPLs. Fig. 2A shows the SPR peak at 563nm. B Plot of $(\alpha h\nu)^{1/2}$ vs photon energy; the bandgap of as synthesized Cu-NPLs is determined from the intercept of the straight line at $\alpha = 0$, which is found to be 2.1 eV. Cu-NPLs were dissolved in DMF and DMF was used as a reference.

https://doi.org/10.1016/j.heliyon.2018.e01077

$$\alpha = \frac{1}{d} Ln\left(\frac{1}{T}\right) \tag{1}$$

where d is the thickness (in cm) of the sample, and T is the transmitted intensity. The bandgap energy of the synthesized Cu nanoparticles was determined using the Tauc relation (Eq. 2).

$$\alpha h\nu = A_o\left(h\nu - E_g\right)^m \tag{2}$$

where hν is the photon energy, m is assumed values of 1/2 and 2 for direct and indirect transitions respectively. A_o is an energy independent constant having values between 1×10^5 and 1×10^6 (cm. eV)$^{-1}$ [36,37]. The value of the energy bandgap (E_g = 2.1 eV) was calculated by extrapolating the linear portion of the plot of $(\alpha h\nu)^{1/2}$ vs. hν (Fig. 2B).

Furthermore, copper exhibits visible photoluminescence due to its surface-enhanced optical phenomenon and the *sp*-conduction band to *d*-band transition [38]. The electronic structure of copper explains the photoluminescence behavior where *3d* valence and *4sp* conduction electrons play a significant role for the photoluminescence. The recombination of the electron-hole pair between *d*-band and *sp*-conduction band followed by initial electronic relaxation is responsible for this photoluminescence behavior. The photoluminescence spectrum of as-prepared Cu-NPLs (Fig. 3) exhibits an excited peak at 562 nm (2.1 eV). The excitation spectrum was found to match with λ_{max} of the reaction medium (SPR at 563 nm). Due to the possibility that the reduction of the Cu^{2+} can produce the preferential formation of copper oxide over Cu^0, X-ray diffraction has been carried out to confirm the chemical identity of the biosynthesized Cu-NPLs.

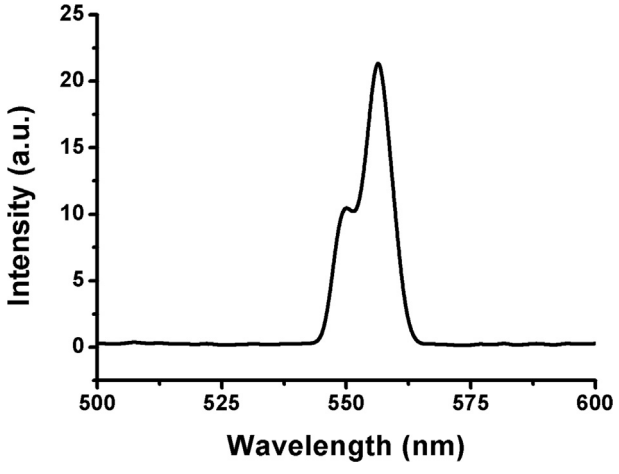

Fig. 3. The photoluminescence spectrum of as-prepared Cu-NPLs exhibits an excited peak at 562 nm.

https://doi.org/10.1016/j.heliyon.2018.e01077

3.3. X-ray diffraction

XRD analysis is a very useful tool in identifying the structure of the metallic nanopowders. The XRD pattern was scanned for the scanning angle of 20−80°. The crystalline nature of Cu-NPLs was confirmed by the peaks obtained in XRD diffraction pattern. Diffraction lines of Cu-NPLs are very sharp (Fig. 4); where three distinct peaks are observed at 2θ values 43.35, 50.50 and 74.21° corresponding to (111), (200) and (220) Miller indices. Study of standard data JCPDS (File No.04-014-0265) confirmed that the as-synthesized materials are cubic Cu phase and are in a good agreement with the standard peak positions of copper crystals [39, 40]. No peaks of impurity were observed, suggesting the high purity Cu-NPLs. The sharpness indicates the crystalline nature of the as-prepared Cu nanostructure. Moreover, the average size of the Cu-NPLs (27.6 nm) is estimated by applying Scherer's formula; $D = 0.9\lambda/(\cos\theta)$, $\lambda = 1.54056\ ^{0}A$, β is full width in radians at half maximum of the peak. XRD provided a significant evidence for the complete reduction of Cu^{2+} ions resulting in the production of metallic copper. Due to XRD measurement limitations, TEM and SEM were utilized to obtain more information about the shape, and size of the as-prepared Cu-NPLs.

3.4. Size and morphology analyses (TEM and SEM)

Through transmission electron microscopy (TEM), it was easy to observe the shape and particle size of Cu-NPLs. The obtained Cu particles exhibited spherical morphology with different particle diameters ranged from 4.7 to 17.4 nm (Fig. 5); TEM micrographs show nanoparticles with spherical and semispherical forms with well-dispersed regions and others with agglomeration. Moreover, the TEM

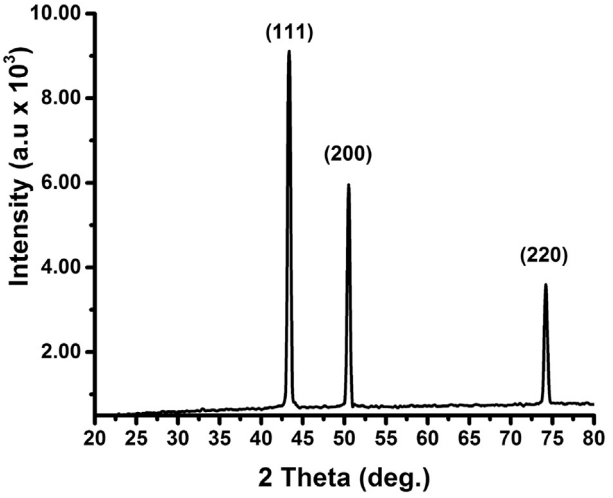

Fig. 4. XRD powder pattern of biosynthesized Cu nanoparticles; Bragg's reflections are observed with values of 43.35, 50.50 and 74.21° representing (1 1 1), (2 0 0) and (2 2 0) planes of the FCC structure of Cu^{0}. Cu-NPLs are highly pure with no traces of copper oxide found on the sample surface.

https://doi.org/10.1016/j.heliyon.2018.e01077

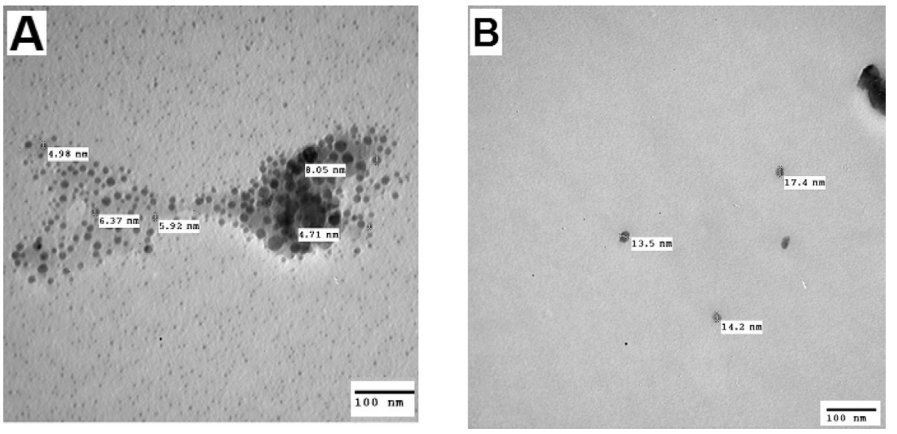

Fig. 5. Selected TEM images of biosynthesized Cu-NPLs. (A) TEM image shows Cu-NPLs with spherical and semispherical forms with well-dispersed regions and others with agglomeration. (B) TEM image confirmed that Cu-NPLs are in nano range.

images clearly show that Cu-NPLs, formed by the reduction of copper ions using fresh aqueous *Tilia* extract, are spherical in appearance. The organic shell plays the significant role of protecting metallic Cu nanoparticles against chemical oxidation which makes them stable and appropriate for coatings or biotechnology applications. The nanoparticles predominately adopt a spherical morphology and they are often agglomerated into small aggregates. These results are consistent with that of FTIR and XRD studies where the phenolic compounds and flavonoids can facilitate the bioreduction of Cu^{2+} ions to Cu^{0} nanoparticles.

Scanning electron microscopy (SEM) provided further insight into the surface morphology of the Cu-NPLs. The typical SEM images reveal that the product mainly consists of particle-like Cu-NPLs crowded together to look like collective cauliflower (Fig. 6A). Further observations with higher magnification reveal that these crowded Cu-NPLs are groups of smaller nanocubes which exhibit shaped-cubic structures with good uniformity (Fig. 6B).

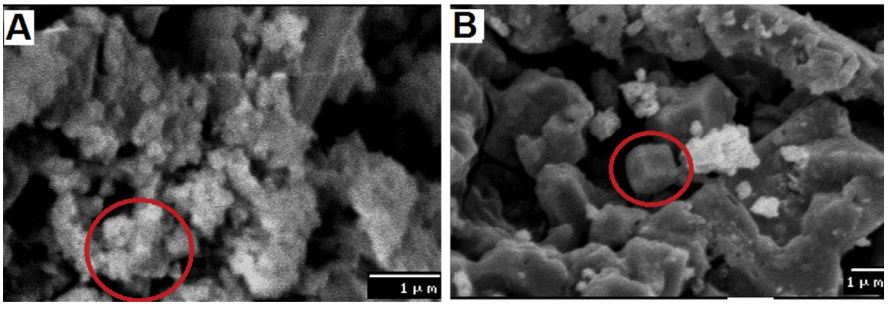

Fig. 6. Selected SEM images of cube shaped Cu-NPLs. (A) SEM image displays Cu-NPLs look like collective cauliflower. (B) SEM image shows shaped-cubic structures with good uniformity.

https://doi.org/10.1016/j.heliyon.2018.e01077

3.5. Electrical conductivity measurement

The electrical conductivity of the Cu-NPLs samples in the temperature range 40−320K was determined; following the Arrhenius model [41]. Arrhenius plot of log(σ) vs 1/T, where σ is the electrical conductivity and T is temperature (K), has been shown in Fig. 7. The slope gives information about activation energy. The Cu-NPLs exhibit high electrical conductivity value (1.04×10^{-6} S cm^{-1}) at T = 120 K. The variation of electrical conductivity with temperature was investigated and it indicated the semiconducting nature of the Cu-NPLs with an activation energy = 0.3 eV in the experimental temperature range. This proves that Cu-NPLs are highly electrically conducting material. Such highly conductive Cu-NPLs may have applications in electronic and energy storage applications.

3.6. Anticancer activity

The main aim of chemotherapy is to remove specifically cancerous cells. Most of the chemotherapeutic agents act non-specifically and hence harming both normal and cancer cells. It was reported that compounds of natural origin have been the main source for the treatment of many forms of cancer and has become an attractive source of new therapeutic agents that can be used for the management of cancer [42]. Cu-NPLs are developing more important roles as therapeutic agents for cancers with the improvement of eco-friendly synthesis methods [43]. The present *in-vitro* study also shows the anti-tumor efficacy of Cu-NPLs on human colon cancer Caco-2 cells, human hepatic cancer HepG2 cells and human breast cancer Mcf-7 cells. Cytotoxicity

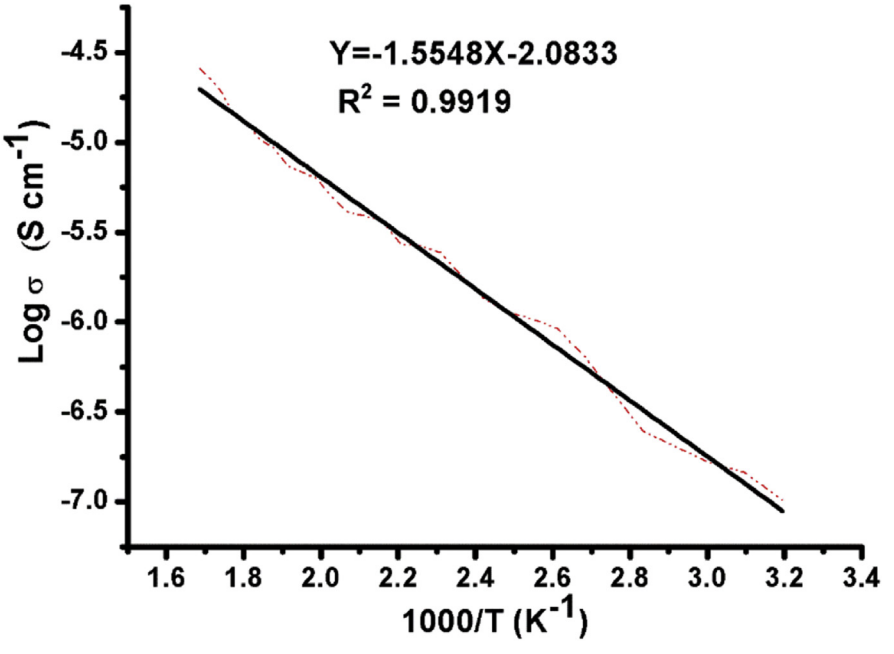

Fig. 7. Arrhenius plot of electrical conductivity (σ) vs. 1/Temperature (K^{-1}) for Cu-NPLs.

https://doi.org/10.1016/j.heliyon.2018.e01077

in vitro studies of Cu-NPLs was carried out on Caco2, HepG-2, and Mcf-7 cell lines by MTT dye conversion assay. This shows that Cu-NPLs hold an excellent biocompatibility. Concerning human colon cancer Caco2 cells, the present investigation conducted that IC_{50} for Cu-NPLS was 11.21 μg. It is noted that Cu-NPLs resulted in a dose-dependent growth inhibition in Caco-2 cells. Concerning human hepatic cancer HepG2 cells, the current results shows IC_{50} for Cu-NPLs was 19.88 μg. Finally, human breast cancer Mcf-7 cells display that IC_{50} for Cu-NPLs was 12.21 μg (Fig. 8).

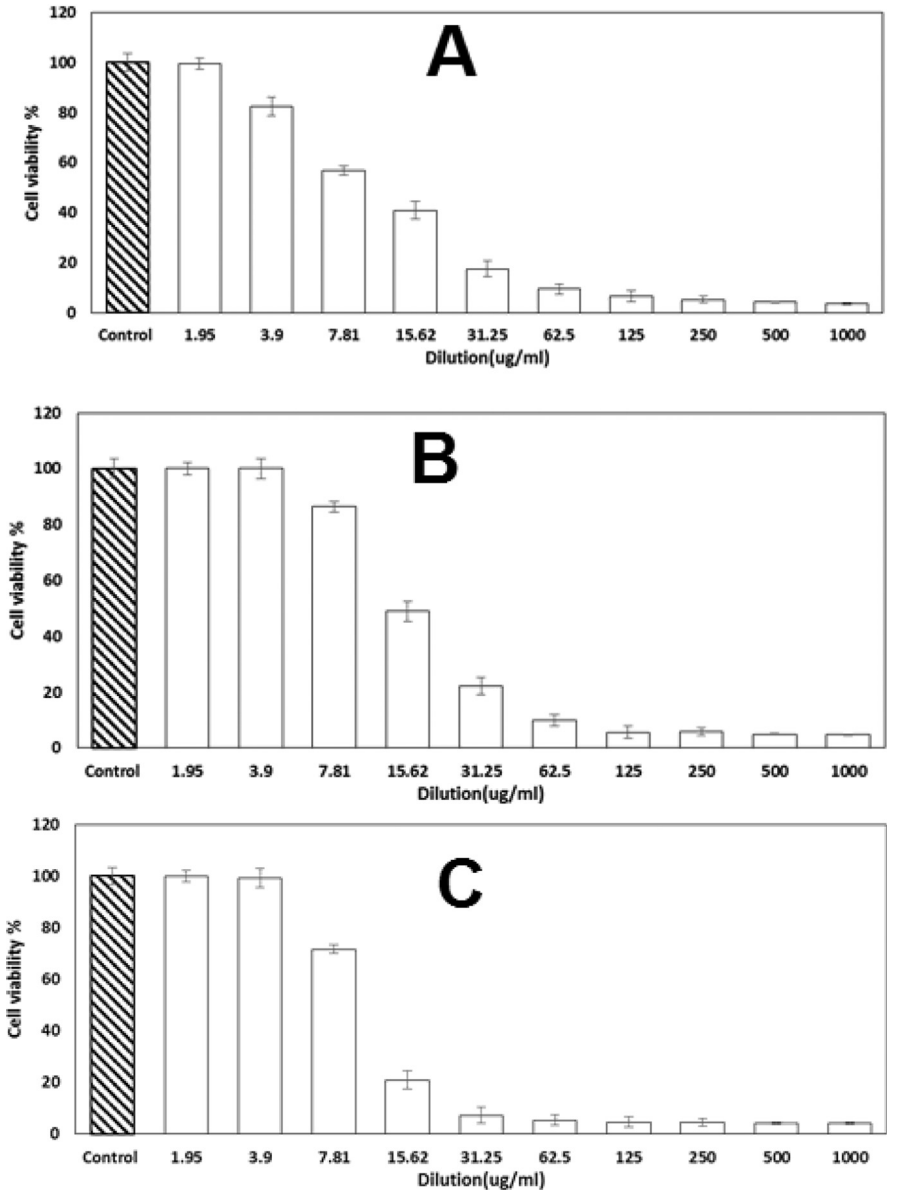

Fig. 8. Effect of Cu-NPLs on human breast cancer MCF-7 cells (A), on human hepatic cancer HepG2 cells (B) and on human colon cancer Caco-2 cells (C) at different concentrations.

https://doi.org/10.1016/j.heliyon.2018.e01077

The results revealed Cu-NPLS are potent anticancer and they significantly enhanced the growth inhibition for all cell lines of investigation, as indicated by marking from IC_{50} values against all cells of the investigation. The green-synthesized Cu-NPLs using *Tilia* extracts have potential applications in the biomedical field and this simple procedure has several advantages such as cost-effectiveness, compatibility for medical and pharmaceutical applications.

3.7. Antimicrobial activity

Nanoparticles have the properties of high surface/volume ratio, small size and high dispersion, which allow them to interact with microbial surfaces. The large surface area of the Cu-NPLs enhances their interaction with the microbes to carry out broad-spectrum antimicrobial activities [44]. However, the few reports on antimicrobial studies of Cu-NPLs proved the effectiveness of Cu-NPLs against various pathogenic microorganisms [1,45]. To study the antibacterial activity of Cu-NPLs, 4 types of bacteria were chosen. The cells of the bacteria could incubate overnight for 24h in growth medium, containing different concentrations of Cu-NPLs. Antibacterial activity against the selected microorganisms (Gram-positive/Gram-positive bacteria) is represented with zones of inhibition (Fig. 9). The values of the zone of inhibition are depicted in Fig. 10.

All Gram-negative & Gram-positive bacteria show good sensitivity towards the green synthesized Cu-NPLs over the concentration range (25−200 μg/mL). In the

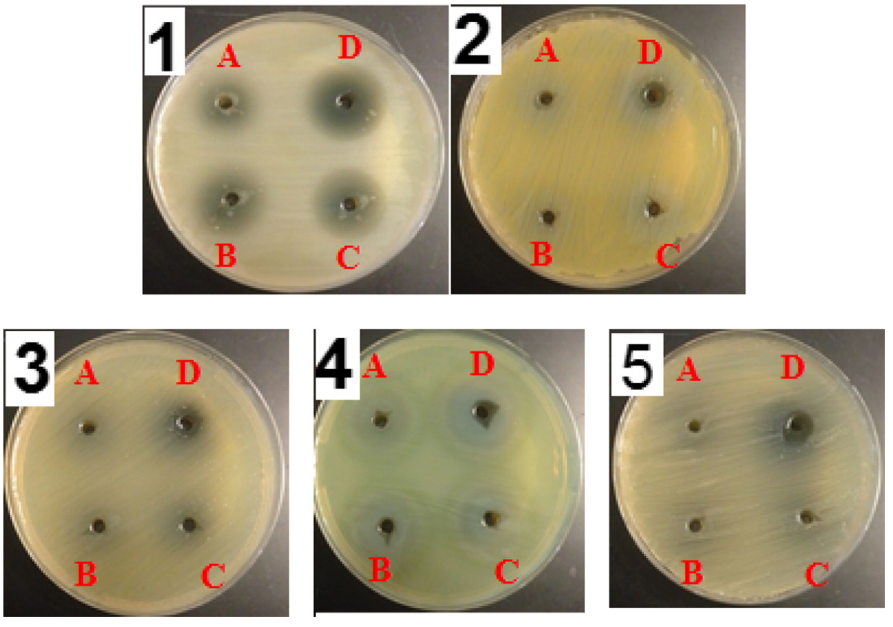

Fig. 9. Antibacterial activity of Cu-NPLs solutions against (1) *B. subtilis*, (2) *S. aureus* (3) *E. coli*, and (4) *P. aeruginosa*. (5) Antifungal activity of Cu-NPLs solution against *Candida albicans*. the concentration of the Cu-NPLs (A = 25, B = 50, C = 100, and D = 200 μg/mL).

https://doi.org/10.1016/j.heliyon.2018.e01077

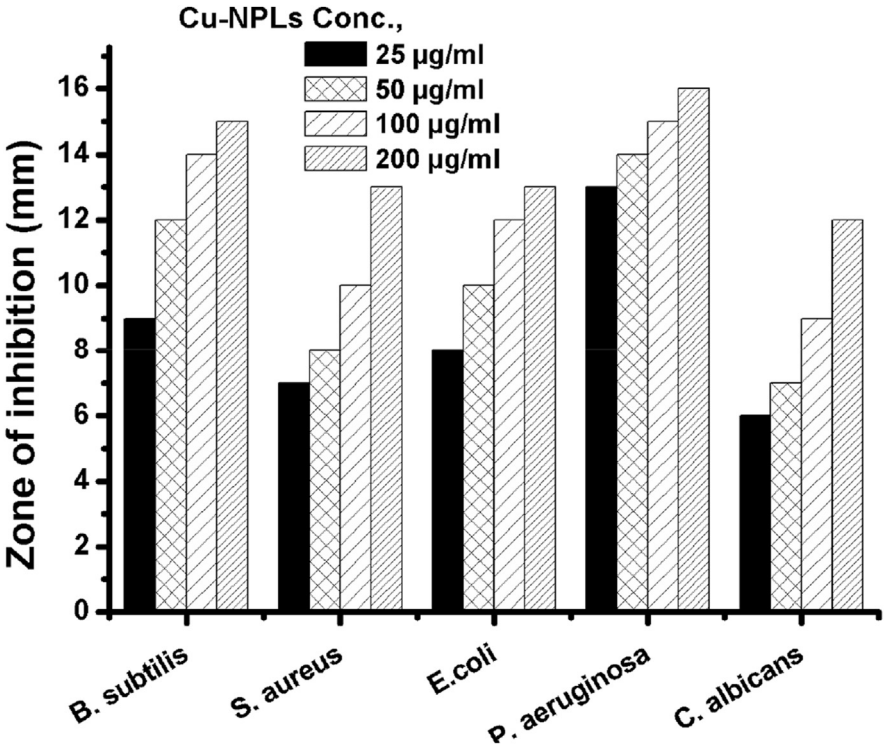

Fig. 10. Antibacterial and antifungal activities of the biosynthesis Cu-NPLs against *B. subtilis*, *S. aureus*, *E. coli*, *P. aeruginosa*, and *C. albicans. The* Cu-NPLs showed more inhibitory activity in bacteria than the fungus. *P. aeruginosa* exhibited the highest mean zone of inhibition in Cu-NPLs.

case of negative control, the absence of a clear zone indicated that both DMSO and the aqueous liquid extract of *Tilia* had no antibacterial or antifungal effect. Fig. 9 shows that as the concentration of the Cu-NPLs (A = 25, B = 50, C = 100, and D = 200 µg/mL) increases, the antibacterial activity also increases. This proves the direct proportionality between the concentration and antibacterial activity as well. Zhang *et al* previously showed that aqueous extract of *Thalia* roots can significantly inhibit the growth of *Aphanizomenon Flos-aquae and Microcystis. aeruginosa* [46].

In a similar manner, antifungal activity was observed toward *Candida albicans* (Fig. 9E). In case of standard positive control; Cefepime hydrochloride monohydrate L-arginine, antifungal standard Fluconazole and suspension of biosynthesized Cu-NPLs exhibited a clear zone (Fig. 11).

The appearance of a clear zone (or inhabitation zone) proved that there was no growth of bacteria or fungi on the plate at these places. This shows the mechanism of interaction of biosynthesized Cu-NPLs which can be due to the smaller particle size/high surface area of Cu-NPLs which adsorbed on the surface of the microorganism's cell wall. This led to the destruction and disruption of cell wall killing the human pathogens by their resistance effect property of biosynthesized Cu-NPLs

https://doi.org/10.1016/j.heliyon.2018.e01077

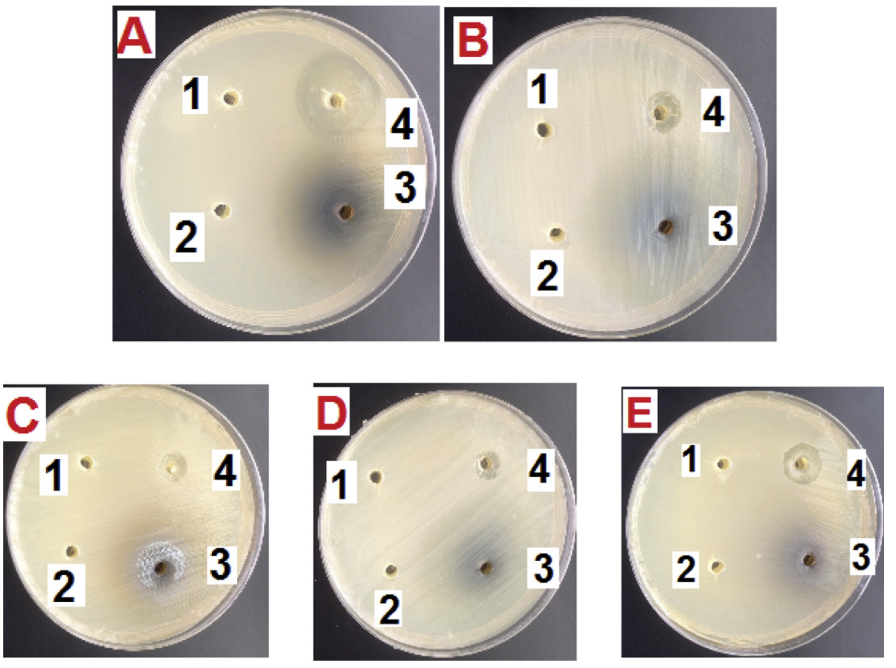

Fig. 11. Antimicrobial activities of Cu-NPLs (100 μg/ml) against (A) *B. subtilis*, (B) *S. aureus* (C) *E. coli* (D) *P. aeruginosa and* (E) *C. albicans*. The numbering refers to: (1) DMSO, (2) *Tilia* extract, (3) Cu-NPLs (100 μg/ml) and (4) antibacterial Cefipime (Fig. 11A–D) and antifungal–Fluconazole (Fig. 11E).

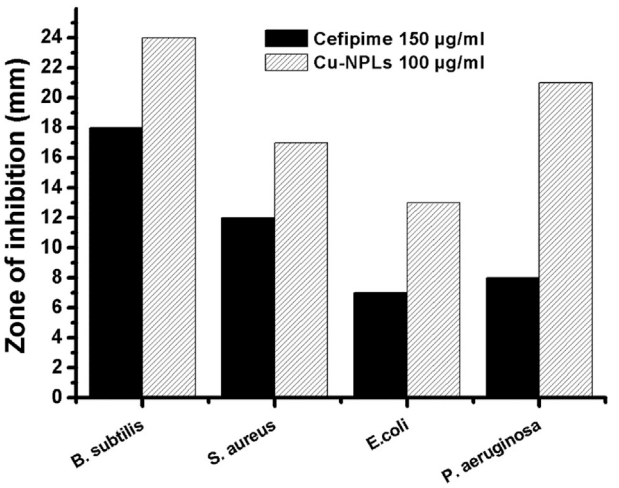

Fig. 12. Antibacterial activity of Cu-NPLs suspension (100 μg/ml) against *Bacillus*, *S. aureus*, *E. coli*, and *P. aeruginosa* and antibacterial Cefipime (150 μg/ml) suggesting that the Cu-NPLs are effective antibacterial and antibiotic agents.

against these types of micro-organisms. The efficacy of biosynthesized Cu-NPLs as an antimicrobial was determined by the diameter of the clear zone; by increasing the diameter the efficacy increases (Fig. 12).

https://doi.org/10.1016/j.heliyon.2018.e01077

Finally, the antimicrobial studies indicated that the use of Cu-NPLs can be pursued as an alternative strategy to antibiotics for reducing bacterial adhesion. Compared with the drug Cefipime (150μg), it was evident that of Cu-NPLs (100 μg) is much more effective against *Bacillus*, *S. aureus*, *E. coli*, and *P. aeruginosa*. Zones of inhibition of Cefipime were 18, 12, 7 and 8 mm, respectively (Fig. 12). The Cu-NPLs showed an effective broad-spectrum antibacterial activity. Further, the Cu-NPLs at 100 μg, produced a higher antimicrobial effect (14 mm) than the Fluconazole (75 μg/mL) in the inhibition of the growth of *B. subtilis* (9mm).

4. Conclusions

Convenient and eco-friendly method for the preparation of Cu-NPLs using biologically reducing $CuSO_4.5H_2O$ with an aqueous *Tilia* extract was developed. The use of *Tilia* extracts for the synthesis of Cu-NPLs was investigated for the first time. *Tilia* extracts function as an excellent reducing and capping agent. The green-synthesized Cu-NPLs were characterized using FTIR, UV-vis, PL, XRD, TEM and SEM techniques. Formation of Cu-NPLs was indicated by changes in the color of the solution from blue to brown due to the excitation of surface plasmon vibration. UV-vis of Cu-NPLs showed an SPR characteristic peak at 563 nm (energy bandgap = 2.1 eV). The photoluminescence spectrum of Cu-NPLs exhibited an excited peak at 562 nm. XRD confirmed the crystalline character of Cu-NPLs. The electrical conductivity of the Cu-NPLs was 1.04×10^{-6} S cm^{-1} (at 120 K). The prepared Cu-NPLs were predominantly spherical in nature with an average particle size of 4.7−17.4 nm. Furthermore, the Cu-NPLs exhibited effective antibacterial and antifungal activities against *Bacillus*, *S. aureus*, *E. coli*, *P. aeruginosa*, and *Candida albicans* respectively. *In vitro* cytotoxic activity studies were done on Caco-2, HepG2 and Mcf-7 cells using MTT assay. Based on the antitumor efficacy, the results showed that Cu-NPLs have a potent cytotoxic activity against Caco-2, HepG2, and Mcf-7 cells. The results suggested that biosynthesized Cu-NPLs that utilize extracts of *Tilia* are a promising nanomaterial in electronic devices and they may be used for the therapeutic applications of ailments such as cancer.

Declarations

Author contribution statement

Reda Hassanien: Conceived and designed the experiments; Analyzed and interpreted the data; Wrote the paper.

Dalal Z. Husein: Conceived and designed the experiments; Contributed reagents, materials, analysis tools or data.

Mostafa F. Al-Hakkani: Performed the experiments.

https://doi.org/10.1016/j.heliyon.2018.e01077

Funding statement

This research did not receive any specific grant from funding agencies in the public, commercial, or not-for-profit sectors.

Competing interest statement

The authors declare no conflict of interest.

Additional information

No additional information is available for this paper.

Acknowledgements

The authors present great thanks to New Valley University for supporting this work under its scientific projects.

References

[1] A. Schröfel, G. Kratošová, I. Šafařík, M. Šafaříková, I. Raška, L.M. Shor, Applications of biosynthesized metallic nanoparticles − a review, Acta Biomater. 10 (2014) 4023−4042.

[2] J.R. Peralta-Videa, Y. Huang, J.G. Parsons, L. Zhao, L. Lopez-Moreno, J.A. Hernandez-Viezcas, J.L. Gardea-Torresdey, Plant-based green synthesis of metallic nanoparticles: scientific curiosity or a realistic alternative to chemical synthesis? Nanotechnol. Environ. Eng. 1 (2016) 4.

[3] Z. Vaseghi, A. Nematollahzadeh, O. Tavakoli, Green methods for the synthesis of metal nanoparticles using biogenic reducing agents: a review, Rev. Chem. Eng. (2017).

[4] M. Rafique, A.J. Shaikh, R. Rasheed, M.B. Tahir, H.F. Bakhat, M.S. Rafique, F. Rabbani, A review on synthesis, characterization and applications of copper nanoparticles using green method, Nano 12 (2017) 1750043.

[5] M. Nasrollahzadeh, S.M. Sajadi, Green synthesis of copper nanoparticles using Ginkgo biloba L. leaf extract and their catalytic activity for the Huisgen [3+2] cycloaddition of azides and alkynes at room temperature, J. Colloid Interface Sci. 457 (2015) 141−147. Epub 2015 Jul 3.

[6] Z. Issaabadi, M. Nasrollahzadeh, S.M. Sajadi, Green synthesis of the copper nanoparticles supported on bentonite and investigation of its catalytic activity, J. Clean. Prod. 142 (2017) 3584−3591.

https://doi.org/10.1016/j.heliyon.2018.e01077

[7] Q. Yao, Z.H. Lu, Z. Zhang, X. Chen, Y. Lan, One-pot synthesis of core-shell Cu@SiO2 nanospheres and their catalysis for hydrolytic dehydrogenation of ammonia borane and hydrazine borane, Sci. Rep. 4 (2014).

[8] M. Ismail, S. Gul, M. Khan, M.A. Khan, A.M. Asiri, S.B. Khan, Green synthesis of zerovalent copper nanoparticles for efficient reduction of toxic azo dyes Congo red and methyl orange, Green Process. Synth. (2018).

[9] Z. Wang, B. Chen, A.L. Rogach, Synthesis, optical properties and applications of light-emitting copper nanoclusters, Nanoscale Horizons 2 (2017) 135−146.

[10] Y. Lee, J.-r. Choi, K.J. Lee, N.E. Stott, D. Kim, Large-scale synthesis of copper nanoparticles by chemically controlled reduction for applications of inkjet-printed electronics, Nanotechnology 19 (2008) 415604. http://stacks.iop.org/0957-4484/19/i=41/a=415604.

[11] V. Abhinav K, V.K. Rao R, P.S. Karthik, S.P. Singh, Copper conductive inks: synthesis and utilization in flexible electronics, RSC Adv. 5 (2015) 63985−64030.

[12] N.A. Dhas, C.P. Raj, A. Gedanken, Synthesis, characterization, and properties of metallic copper nanoparticles, Chem. Mater. 10 (1998) 1446−1452.

[13] H. Choi, S.-H. Park, Seedless growth of free-standing copper nanowires by chemical vapor deposition, J. Am. Chem. Soc. 126 (2004) 6248−6249.

[14] L. Huang, H. Jiang, J. Zhang, Z. Zhang, P. Zhang, Synthesis of copper nanoparticles containing diamond-like carbon films by electrochemical method, Electrochem. Commun. 8 (2006) 262−266.

[15] P.V. Krasovskii, A.V. Samokhin, A.A. Fadeev, N.V. Alexeev, Thermal evolution study of nonmetallic impurities and surface passivation of Cu nanopowders produced via a DC thermal plasma synthesis, Adv. Powder Technol. 27 (2016) 1669−1676.

[16] C.F. Monson, A.T. Woolley, DNA-templated construction of copper nanowires, Nano Lett. 3 (2003) 359−363.

[17] J. Xiong, Y. Wang, Q. Xue, X. Wu, Synthesis of highly stable dispersions of nanosized copper particles using l-ascorbic acid, Green Chem. 13 (2011) 900−904.

[18] N.V. Surmawar, S.R. Thakare, N. Khaty, One-pot, single step green synthesis of copper nanoparticles: SPR nanoparticles, Int. J. Green Nanotechnol. 3 (2011) 302−308.

[19] Y. Yang, Z.-H. Lu, Y. Hu, Z. Zhang, W. Shi, X. Chen, T. Wang, Facile in situ synthesis of copper nanoparticles supported on reduced graphene oxide for

 https://doi.org/10.1016/j.heliyon.2018.e01077

hydrolytic dehydrogenation of ammonia borane, RSC Adv. 4 (2014) 13749−13752.

[20] S. Shoeibi, P. Mozdziak, A. Golkar-Narenji, Biogenesis of selenium nanoparticles using green chemistry, Top. Curr. Chem. 375 (2017) 017−0176.

[21] S.J. Chang, C.A. Tung, B.W. Chen, Y.C. Chou, C.C. Li, Synthesis of non-oxidative copper nanoparticles, RSC Adv. 3 (2013) 24005−24008.

[22] S. Yokoyama, H. Takahashi, T. Itoh, K. Motomiya, K. Tohji, Synthesis of metallic Cu nanoparticles by controlling Cu complexes in aqueous solution, Adv. Powder Technol. 25 (2014) 999−1006.

[23] S. Ahmed, M. Ahmad, B.L. Swami, S. Ikram, A review on plants extract mediated synthesis of silver nanoparticles for antimicrobial applications: a green expertise, J. Adv. Res. 7 (2016) 17−28.

[24] M. Nasrollahzadeh, F. Babaei, P. Fakhri, B. Jaleh, Synthesis, characterization, structural, optical properties and catalytic activity of reduced graphene oxide/copper nanocomposites, RSC Adv. 5 (2015) 10782−10789.

[25] K. Cheirmadurai, S. Biswas, R. Murali, P. Thanikaivelan, Green synthesis of copper nanoparticles and conducting nanobiocomposites using plant and animal sources, RSC Adv. 4 (2014) 19507−19511.

[26] A.K. Mittal, Y. Chisti, U.C. Banerjee, Synthesis of metallic nanoparticles using plant extracts, Biotechnol. Adv. 31 (2013) 346−356.

[27] M. Shah, D. Fawcett, S. Sharma, S.K. Tripathy, G.E.J. Poinern, Green synthesis of metallic nanoparticles via biological entities, Materials 8 (2015) 7278−7308.

[28] S.C. Capaldi Arruda, A.L. Diniz Silva, R. Moretto Galazzi, R. Antunes Azevedo, M.A. Zezzi Arruda, Nanoparticles applied to plant science: a review, Talanta 131 (2015) 693−705.

[29] A. Karioti, L. Chiarabini, A. Alachkar, M. Fawaz Chehna, F.F. Vincieri, A.R. Bilia, HPLC−DAD and HPLC−ESI-MS analyses of Tiliae flos and its preparations, J. Pharmaceut. Biomed. Anal. 100 (2014) 205−214.

[30] L.V. Rubinstein, R.H. Shoemaker, K.D. Paull, R.M. Simon, S. Tosini, P. Skehan, D.A. Scudiero, A. Monks, M.R. Boyd, Comparison of in vitro anticancer-drug-screening data generated with a tetrazolium assay versus a protein assay against a diverse panel of human tumor cell lines, J. Natl. Cancer Inst. 82 (1990) 1113−1118.

[31] M. Nasrollahzadeh, S.M. Sajadi, M. Khalaj, Green synthesis of copper nanoparticles using aqueous extract of the leaves of Euphorbia esula L and their

 https://doi.org/10.1016/j.heliyon.2018.e01077

catalytic activity for ligand-free Ullmann-coupling reaction and reduction of 4-nitrophenol, RSC Adv. 4 (2014) 47313–47318.

[32] H. Reda, A.F.A.-S. Said, Š. Lidija, L. Ross, G.W. Nicholas, H. Andrew, R.H. Benjamin, Smooth and conductive DNA-templated Cu 2 O nanowires: growth morphology, spectroscopic and electrical characterization, Nanotechnology 23 (2012) 075601.

[33] M.A. Shoeib, O.E. Abdelsalam, M.G. Khafagi, R.E. Hammam, Synthesis of Cu2O nanocrystallites and their adsorption and photocatalysis behavior, Adv. Powder Technol. 23 (2012) 298–304.

[34] R. Hassanien, M.M. Almaky, A. Houlton, B.R. Horrocks, Preparation and electrical properties of a copper-conductive polymer hybrid nanostructure, RSC Adv. 6 (2016) 99422–99432.

[35] A. Valentini, E. Nappi, M.A. Nitti, Influence of the substrate reflectance on the quantum efficiency of thin CsI photocathodes, Nucl. Instrum. Methods Phys. Res. Sect. A Accel. Spectrom. Detect. Assoc. Equip. 482 (2002) 238–243.

[36] M. Dutta, S. Mridha, D. Basak, Effect of sol concentration on the properties of ZnO thin films prepared by sol–gel technique, Appl. Surf. Sci. 254 (2008) 2743–2747.

[37] E.F. Keskenler, G. Turgut, S. Doğan, Investigation of structural and optical properties of ZnO films co-doped with fluorine and indium, Superlattice. Microst. 52 (2012) 107–115.

[38] Y. Suresh, S. Annapurna, G. Bhikshamaiah, A.K. Singh, Green luminescent copper nanoparticles, IOP Conf. Ser. Mater. Sci. Eng. 149 (2016) 012187.

[39] D. Mott, J. Galkowski, L. Wang, J. Luo, C.-J. Zhong, Synthesis of size-controlled and shaped copper nanoparticles, Langmuir 23 (2007) 5740–5745.

[40] R. Zhou, X. Wu, X. Hao, F. Zhou, H. Li, W. Rao, Influences of surfactants on the preparation of copper nanoparticles by electron beam irradiation, Nucl. Instrum. Methods Phys. Res. Sect. B Beam Interact. Mater. Atoms 266 (2008) 599–603.

[41] M. Gosh, A. Barman, A.K. Meikap, S.K. De, S. Chatterjee, Hopping transport in HCl doped conducting polyaniline, Phys. Lett. 260 (1999) 138–148.

[42] A. Rayan, J. Raiyn, M. Falah, Nature is the best source of anticancer drugs: indexing natural products for their anticancer bioactivity, PLoS One 12 (2017) e0187925-e0187925.

 https://doi.org/10.1016/j.heliyon.2018.e01077

[43] S. Harne, A. Sharma, M. Dhaygude, S. Joglekar, K. Kodam, M. Hudlikar, Novel route for rapid biosynthesis of copper nanoparticles using aqueous extract of Calotropis procera L. latex and their cytotoxicity on tumor cells, Colloids Surfaces B Biointerfaces 95 (2012) 284–288.

[44] S. Shende, A.P. Ingle, A. Gade, M. Rai, Green synthesis of copper nanoparticles by Citrus medica Linn. (Idilimbu) juice and its antimicrobial activity, World J. Microbiol. Biotechnol. 31 (2015) 865–873.

[45] S. Shiravand, F. Azarbani, Phytosynthesis, characterization, antibacterial and cytotoxic effects of copper nanoparticles, Green Chem. Lett. Rev. 10 (2017) 241–249.

[46] T.-t. Zhang, L.-l. Wang, Z.-x. He, D. Zhang, Growth inhibition and biochemical changes of cyanobacteria induced by emergent macrophyte Thalia dealbata roots, Biochem. Syst. Ecol. 39 (2011) 88–94.

https://doi.org/10.1016/j.heliyon.2018.e01077